The Astrophysical Journal Letters, 851:L27 (6pp), 2017 December 20 https://doi.org/10.3847/2041-8213/aa9b2e

Discovery of Periodic Dips in the Brightest Hard X-Ray Source of M31 with EXTraS

Martino Marelli[1,2], Andrea Tiengo[1,2,3], Andrea De Luca[2,3], David Salvetti[2], Luca Saronni[4], Lara Sidoli[2], Adamantia Paizis[2], Ruben Salvaterra[2], Andrea Belfiore[1,2], Gianluca Israel[5], Frank Haberl[6], and Daniele D'Agostino[7]
[1] Scuola Universitaria Superiore IUSS Pavia, Piazza della Vittoria 15, I-27100 Pavia, Italy; marelli@lambrate.inaf.it
[2] INAF—Istituto di Astrofisica Spaziale e Fisica Cosmica Milano, Via E. Bassini 15, I-20133 Milano, Italy
[3] INFN—Istituto Nazionale di Fisica Nucleare, Sezione di Pavia, Via Bassi 6, I-27100 Pavia, Italy
[4] Università degli Studi di Milano, Via Festa del Perdono 7, I-20122 Milano, Italy
[5] INAF—Osservatorio Astronomico di Roma, Via Frascati 33, I-00040 Monteporzio Catone, Italy
[6] Max-Planck-Institut fur extraterrestrische Physik, Giessenbachstrase, D-85748 Garching, Germany
[7] Istituto di Matematica Applicata e Tecnologie Informatiche CNR, Via dei Marini 6, I-16149 Genova, Italy
Received 2017 October 4; revised 2017 November 13; accepted 2017 November 14; published 2017 December 11

Abstract

We performed a search for eclipsing and dipping sources in the archive of the EXTraS project—a systematic characterization of the temporal behavior of *XMM-Newton* point sources. We discovered dips in the X-ray light curve of 3XMM J004232.1+411314, which has been recently associated with the hard X-ray source dominating the emission of M31. A systematic analysis of *XMM-Newton* observations revealed 13 dips in 40 observations (total exposure time of ∼0.8 Ms). Among them, four observations show two dips, separated by ∼4.01 hr. Dip depths and durations are variable. The dips occur only during low-luminosity states ($L_{0.2-12} < 1 \times 10^{38}$ erg s^{-1}), while the source reaches $L_{0.2-12} \sim 2.8 \times 10^{38}$ erg s^{-1}. We propose that this system is a new dipping low-mass X-ray binary in M31 seen at high inclination (60°–80°); the observed dipping periodicity is the orbital period of the system. A blue *HST* source within the *Chandra* error circle is the most likely optical counterpart of the accretion disk. The high luminosity of the system makes it the most luminous (not ULX) dipper known to date.

Key words: galaxies: bulges – galaxies: individual (M31) – pulsars: general – stars: neutron – X-rays: binaries

Supporting material: machine-readable table

1. Introduction

The Exploring the X-ray Transient and variable Sky (EXTraS) project (De Luca et al. 2016) developed new techniques and tools to extract and describe the timing behavior of X-ray sources. The entire public *XMM-Newton* archive (3XMM catalog, data release 4[8]) was analyzed, obtaining hundreds of parameters to describe the periodic and aperiodic variability of more than 500,000 serendipitous sources, on different timescales (from seconds to years). The results are publicly available, together with detailed documentation.[9] Taking advantage of this improved *XMM-Newton* timing analysis, we performed a systematic search for eclipsing and dipping objects, finding significant dips in the light curves of some observations of 3XMM J004232.1+411314 (XMM0042 hereafter).

XMM0042 is a moderately bright (∼0.2 counts s^{-1}) source observed multiple times by *XMM-Newton* due to its proximity to the M31 bulge. Based on flux and spectral variability studies in the 0.5–10 keV energy band, the source has been classified as an X-ray binary candidate in various *Chandra* and *XMM-Newton* studies (see, e.g., Kong et al. 2002; Stiele et al. 2011). Based on *NuSTAR* data, it has been recently associated with the most prominent source of hard X-rays from M31 (Yukita et al. 2017). The simultaneous *Swift/XRT* and *NuSTAR* spectrum is well fit assuming an accretion disk model with a temperature of ∼0.2 keV and a broken power law, with a photon index of ∼1 and an energy cutoff at ∼18 keV. If XMM0042 is in M31 (784 ± 13 kpc; Stanek & Garnavich 1998), its 0.5–50 keV luminosity is $L_{0.5-50\,\mathrm{keV}} \sim 4 \times 10^{38}$ erg s^{-1}. The most precise X-ray position of XMM0042 comes from *Chandra*, at R.A. (J2000) $00^{h}42^{m}32^{s}.072$, decl. (J2000) +41°13′14.″33 (0.″4, 3σ error; Barnard et al. 2014). *HST* observations revealed 17 possible optical/UV counterparts (Yukita et al. 2017), none of which is compatible with a high-mass donor (>3 $M_{\odot}$).

We collected all the EXTraS results of XMM0042 and applied the same analysis to extract the same products from the most recent observations within the 3XMM catalog, data release 7.[10] Section 2 describes the spectral study we performed, as well as the investigation of the source light curve. The interpretation and discussion of our most relevant results are reported in Section 3, together with a discussion of the nature of the source in the light of these new results.

2. Data Analysis

We searched for all the *XMM-Newton* observations of XMM0042 in the 3XMM catalog DR7. EXTraS data make use of the same filters as the 3XMM catalogs—energy band (0.2–12 keV), pattern, and flags. We selected exposures with the most stable attitude, also excluding the ones with the source partially outside the field of view or on CCD gaps. The observations we analyzed are listed in the machine-readable version of Table 1.

We made use of SAS v.15 to perform a standard analysis from ODF files. For the spectral analysis only, we excluded very high background periods (>40 counts s^{-1} from the PN camera and >15 from MOS1/2 from the entire field of view, in the 0.2–12 keV energy range). Following Yukita et al. (2017) we adopted an absorbed (abundances from Wilms et al. 2000) accretion disk model plus power law (the cutoff energy is ∼17 keV, above our energy range). As in Yukita et al. (2017),

[8] http://xmmssc-www.star.le.ac.uk/Catalogue/3XMM-DR4
[9] http://www.extras-fp7.eu
[10] http://xmmssc.irap.omp.eu/Catalogue/3XMM-DR7/3XMM_DR7.html

Table 1
Dipping Light Curve Parameters

Obs.Num.	OBSID	$N_{\rm dips}$	nhp	$L_{\rm out}$ (10^{38} erg s^{-1})	$T_{\rm min}$ (MJD)	ΔT (ks)	$L_{\rm min}$ (10^{38} erg s^{-1})
9	0405320701	1	6.47×10^{-2}	0.85 ± 0.03	54100.737 ± 0.001	2.87 ± 0.47	0.17 ± 0.09
11	0405320901	1	3.20×10^{-1}	0.93 ± 0.03	54136.287 ± 0.001	3.84 ± 0.48	0.26 ± 0.06
12	0505720201	2	8.56×10^{-1}	0.82 ± 0.02	54463.683 ± 0.001	3.04 ± 0.33	0.08 ± 0.06
…	…	2	…	…	54463.850 ± 0.002	3.36 ± 0.55	0.41 ± 0.06
18	0551690201	2	4.52×10^{-3}	0.86 ± 0.03	54830.223 ± 0.002	4.75 ± 0.64	0.16 ± 0.07
…	…	2	…	…	54830.379 ± 0.004	2.80 ± 1.76	0.22 ± 0.18
22	0551690601	2	8.80×10^{-3}	0.82 ± 0.03	54866.623 ± 0.002	2.19 ± 0.55	0.08 ± 0.02
…	…	2	…	…	54866.791 ± 0.002	2.50 ± 0.82	0.38 ± 0.11
27	0600660601	1	3.14×10^{-1}	0.97 ± 0.03	55229.226 ± 0.002	2.23 ± 0.47	0.49 ± 0.10
30	0650560401	2	1.51×10^{-2}	0.92 ± 0.03	55576.019 ± 0.002	3.36 ± 0.55	0.21 ± 0.09
…	…	2	…	…	55576.186 ± 0.001	5.00 ± 0.56	0.10 ± 0.06
33	0674210201	1	9.60×10^{-2}	1.38 ± 0.03	55923.159 ± 0.004	5.00 ± 1.54	0.99 ± 0.11
35	0674210401	1	3.61×10^{-1}	1.36 ± 0.03	55941.708 ± 0.001	2.83 ± 0.52	0.66 ± 0.12

Note. We report the parameters of the best-fit constant+dips model of dipping *XMM-Newton* light curves of XMM0042 that we analyzed. We show the observation number, number of dips, null hypothesis probability, and the parameters as described in Section 2. More detailed information can be found in the machine-readable table.

Table 2
Best-fit Parameters of the Total PN, MOS1, and MOS2 Spectra of XMM0042

Spectral Model	nhp	$T_{\rm in}$ (keV)	$R_{\rm in}$ (km)	Γ	$N_{\rm pow}$ 10^{-5}	Line$_E$ (keV)	Line$_\sigma$ (keV)	Line$_{\rm norm}$ 10^{-5}
tbabs(diskbb+pow)	1.50×10^{-10}	0.188 ± 0.003	26.5 ± 1.0	0.98 ± 0.01	6.0 ± 0.1	…	…	…
tbabs(gau+diskbb+pow)	4.11×10^{-2}	0.198 ± 0.003	$25.5^{+1.3}_{-1.2}$	0.91 ± 0.01	5.5 ± 0.1	$0.62^{+0.02}_{-0.03}$	$0.15^{+0.02}_{-0.01}$	$-3.6^{+0.6}_{-0.9}$
tbabs(gau+diskbb+pow)	9.49×10^{-3}	0.128 ± 0.005	$10.5^{+1.0}_{-1.1}$	0.98 ± 0.01	6.0 ± 0.1	$0.94^{+0.02}_{-0.03}$	0.20 ± 0.02	$1.8^{+0.4}_{-0.3}$

Note. We report the parameters of best fits obtained using the total PN, MOS1, and MOS2 spectra, as discussed in Section 2. Inner radius has been calculated using a distance of 784 kpc and an inclination i of 70°, where $R_{\rm in} = D_{[10\,{\rm kpc}]}/\sqrt{N_{\rm diskbb} * \sin(i)}$.

(This table is available in its entirety in machine-readable form.)

the column density was fixed to the Galactic value of 7×10^{20} cm^{-2}. Adding together the spectra of all the observations (and correcting for response matrices and effective areas), we obtain a poor fit, with a null hypothesis probability nhp $= 1.5 \times 10^{-10}$, 2312 degrees of freedom (dof). The residuals are structured, with a clear shortage around 0.6 keV and an excess at around 1 keV. The spectrum is well fit either by adding a broad Gaussian emission line at ∼0.95 keV (nhp $= 9.5 \times 10^{-3}$, dof $= 2310$) or a broad Gaussian absorption line at ∼0.6 keV (nhp $= 4.0 \times 10^{-2}$, dof $= 2310$). The best-fitting parameters are reported in Table 2. A contemporaneous fit of all spectra is in agreement with the single-spectra result.

We adopted the total absorbed double-component plus emission line model and parameters in Table 2 to derive the X-ray luminosity for each instrument and observation and exploit the simultaneous observations of PN, MOS1, and MOS2. This was used to obtain hardness ratios in different energy bands for each observation. Figure 1 shows the hardness ratio between 0.2–0.8 keV and 0.8–2 keV bands. The variation with time is apparent (nhp $= 1.6 \times 10^{-11}$, dof $= 39$). Higher-energy band hardness ratio analysis revealed no significant change with time. This suggests some type of variation with time in the thermal component (or in the lines, if present).

EXTraS light curves from different instruments and exposures are binned using the same time bins (a grid of 500 s time bins beginning with the zero *XMM-Newton* reference time); therefore, we calculated the weighted mean, bin by bin, of the luminosity curves from PN and MOS1/2 to obtain the total light curve of each observation. Then, we fit each observation light curve using a constant model. If the fit was not statistically acceptable (3σ), we used a more complex model. We tried this with a linear model and constant-plus-dips model. The last one has four parameters: $T_{\rm min}$ is the time of minimum luminosity, ΔT is the duration of the dip, $L_{\rm min}$ is the minimum luminosity, and $L_{\rm out}$ is the luminosity outside the dip. An f-test (Bevington 1969) was used to confirm the statistical improvement by using the more complex models.

According to our investigation, 29 curves with exposures varying from ∼11 ks to ∼33 ks are constant, five reveal a single dip, and four have two dips, for a total of 13 significant dips. The longest observation (obs.id 0112570101), with a ∼64 ks exposure, is the only one that reveals a linear decrease in luminosity. Only one curve (obs.id 0674210501) is variable at $>4\sigma$ but does not fit with our classification due to the presence of a more complex variability.

Within double-dipping observations, the time interval between dips minima is consistent with being constant (1σ confidence) revealing a periodicity of (14.47 ± 0.12) ks, as is apparent in Figure 2 (the minimum separation in obs.id 0551690201 should be considered as a lower limit because we observe only part of the second dip). Considering a 14.47 ks period, all single-dip observations are characterized by

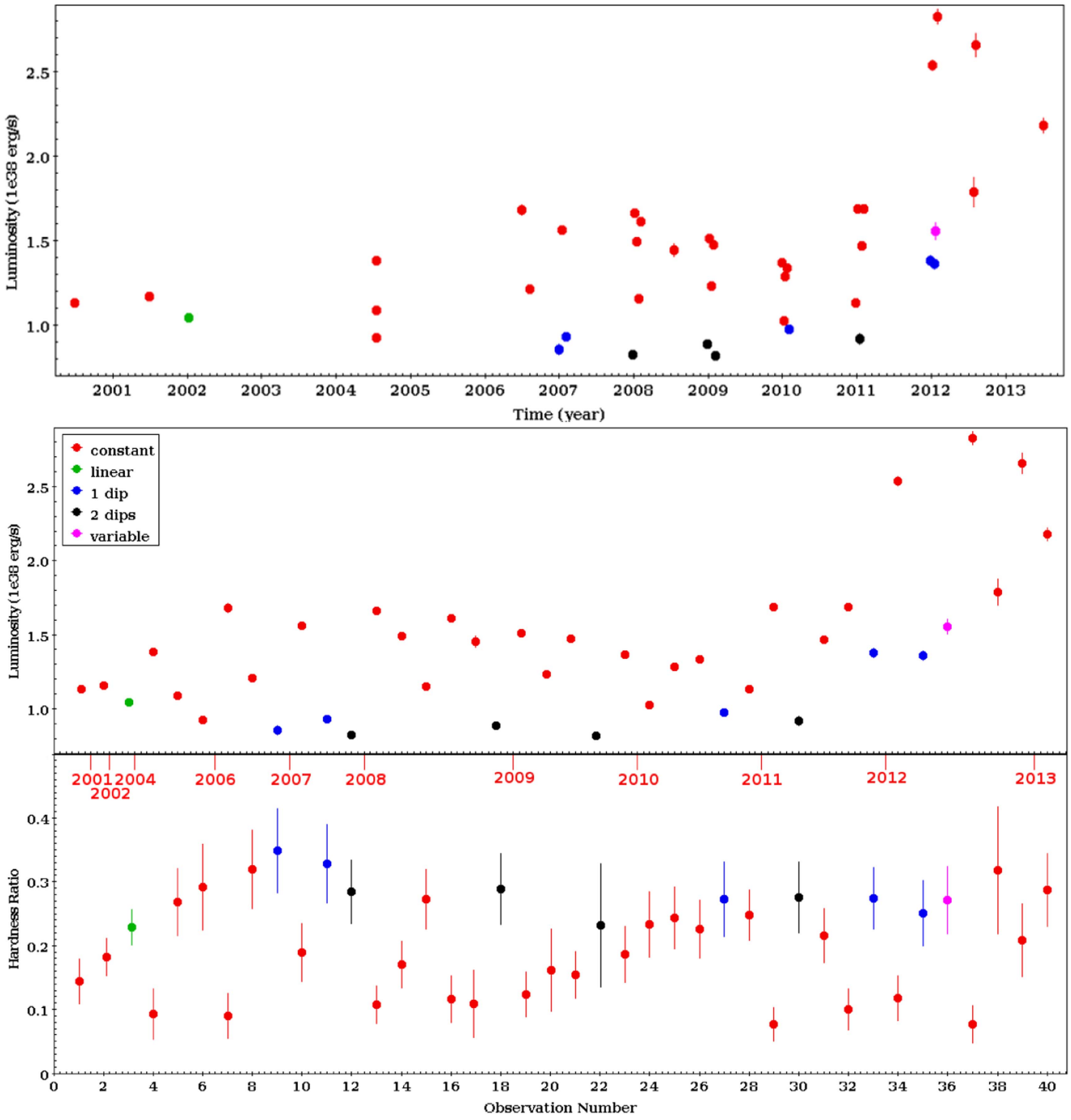

Figure 1. Top panel: persistent X-ray luminosities during the analyzed *XMM-Newton* observations, as reported in Table 1. Different colors mark observations with the light curve best fit by a different model: red for constant, green for linear, magenta for variable, blue for single dip, and black for double dips. Middle panel: we show the same luminosity as in the top panel. The observation number in the *X*-axis allows us to easily associate the observation with the results reported in the machine-readable version of Table 1. Different colors mark observations with the light curve best fit by a different model, as above. Bottom panel: hardness ratio of XMM0042 comparing the 0.2–0.8 keV and 0.8–2 keV energy ranges. The hardness ratio is defined as $(L_{08-2} - L_{02-08})/(L_{08-2} + L_{02-08})$ (see Section 2). Different colors mark observations with the light curve best fit by a different model, as above.

exposures that do not allow for the detection of the previous and following dips. On the other hand, almost all of the observations well fit by a constant model cover more than one period.

Searches for a periodicity using multiple data sets, e.g., with the Lomb–Scargle algorithm (Zechmeister & Kurster 2009) is hampered by the time separation between double-dipping observations.

We also divided the observations with dips in order to isolate the dipping periods from the rest of the observation. We do not detect any significant spectral variation during the dips: a simultaneous fit of spectra of the two data sets, with all the variables chained but a multiplicative factor, results in an acceptable fit (nhp $= 3.0 \times 10^{-2}$, dof $= 1124$). We note that due to the low statistics we would not detect (3σ confidence) variations in the disk temperature and in the photon index smaller than 25% and 10%, respectively.

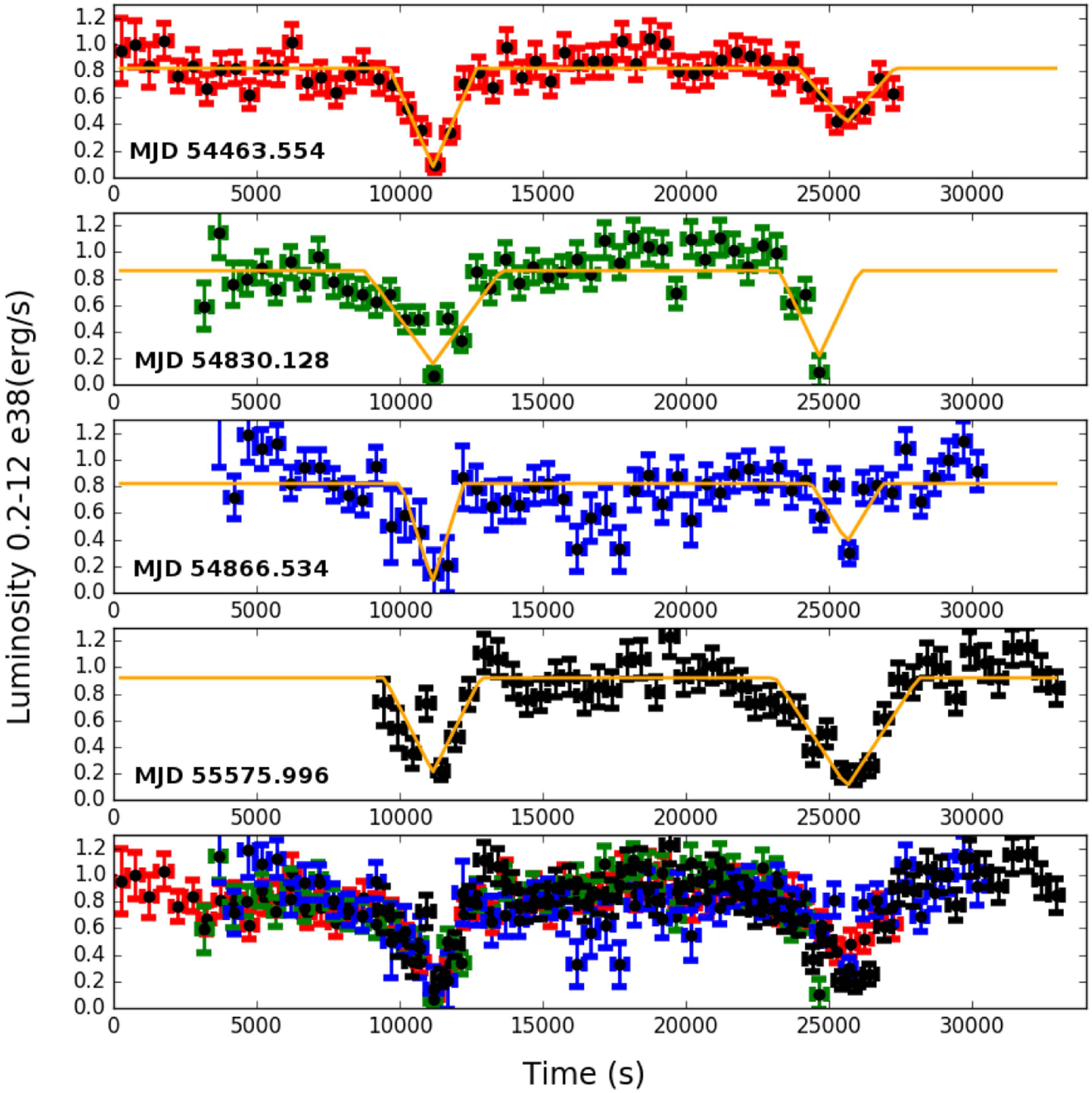

Figure 2. Four *XMM-Newton* luminosity light curves (0.2–12 keV) of XMM0042 where two dips are found (observations 0505720201, 0551690201, 0551690601, and 0650560401, respectively). Each light curve start time is shown in the corresponding panel. They are aligned in order to have the first minimum of the model at the same time. We show the 1σ error on 500 s time bins. The 4 hr period is apparent, as well as the dishomogeneity of the dip profiles. It is also apparent that outside the dips the source luminosity is consistent for all the observations. In the last panel, we show the superimposition of the curves.

The dip duration is variable from ∼2.2 ks to ∼5.0 ks; the minimum luminosity varies from ∼10% to ∼70% of the persistent luminosity. We note that the low statistics prevents us from detecting dips (3σ significance) with a minimum luminosity >75% of the constant luminosity. Dipping observations occur only during low-luminosity states ($L_{0.2-12} < 1 \times 10^{38}$ erg s^{-1}), while observations where we found no dips occur at all possible luminosities ($0.9 \times 10^{38} < L_{0.2-12} < 1.7 \times 10^{38}$ erg s^{-1}) before 2012. Starting from 2012, the source persistent luminosity increases by a factor of ∼2, with luminosities $1.4 \times 10^{38} < L_{0.2-12} < 2.8 \times 10^{38}$ erg s^{-1}. Dipping observations still occur only during low-luminosity states (see Figure 1).

The better spatial resolution of *Chandra* allows us to detect two different sources, about 8″ apart, that contribute to the emission of the *XMM-Newton* XMM0042 source. Hofmann et al. (2013) present an accurate study of the variability of these sources. Source 75 (R.A. (J2000) $00^{h}42^{m}32\overset{s}{.}07$, decl. (J2000) $+41°13'14\overset{''}{.}6$) is the brightest one and varies by a factor of ∼5 during the 14 years of observation (from 1998 to 2012), showing a general increase of the flux with time on a timescale of years. Source 78 (R.A. (J2000) $00^{h}42^{m}32\overset{s}{.}74$, decl. (J2000) $+41°13'11\overset{''}{.}1$) is almost constant, a factor of 10 less luminous than source 75. Hence, we conclude that the flux of XMM0042 and its variability can be ascribed to source 75, with a negligible contribution from source 78.

3. Discussion

We have discovered a diplike modulation in the light curve of XMM0042. These dips occur with a period of 4.01 hr. If the 4.01 hr modulation represents the binary period of XMM0042, the binary separation is $a \sim 10^{11} M_X^{1/3}(1+q)^{1/3}$ cm, where M_X is the mass of the compact object (in solar masses) and q is the mass ratio of the companion star and the compact object. This short orbital separation rules out a high-mass X-ray binary system with a blue supergiant (or a Be main-sequence) companion. This agrees with *HST* observations (Yukita et al. 2017) that exclude high-mass ($>3\,M_\odot$) donors at the location of this source. We note that this period does not exclude an XRB with a Wolf–Rayet donor (Cyg X-3 in our Galaxy has a similar orbital period). However, the light curve of Cyg X-3 is very different from the one of XMM0042 (very stable and quasi-sinusoidal), so we can safely consider that it is more likely a dipping low-mass X-ray binary (LMXB), given the similarities of their orbital light curves.

LMXB systems are known to show dips if the system is viewed relatively close to edge-on, i.e., at a high inclination angle of 60°–80° (Frank et al. 1987): the duration and variability of XMM0042 dips are similar to those seen in some well-known Galactic LMXBs, such as XB 1254-690 and XB 1916-053 (Diaz Trigo et al. 2006). For these Galactic sources the dips have different shapes and are not detected in all the orbital cycles, as we observe for XMM0042. Dips are thought to be due to absorption from the matter in the external region of the accretion disk (White & Swank 1982). The spectral evolution during dips depends on the ionization state of the absorbing material (Diaz Trigo & Boirin 2016). In the case of XMM0042, we do not detect any significant spectral variation possibly due to the low statistics.

Van Paradijs & McClintock (1994) study the optical emission from LMXB disks; if X-rays from the central source are reprocessed by the accretion disk, this implies that the optical luminosity in the V-band M_V scales with the X-ray luminosity and size of the accretion disk. We considered the relation from Van Paradijs & McClintock (1994) between L_X, the orbital period, and M_V, taking into account $L_{\rm Edd} = 2.5 \times 10^{38}$ erg s^{-1} (following Van Paradijs & McClintock 1994), our orbital period of 4.01 hr, and our mean luminosity $L_X = 2 \times 10^{38}$ erg s^{-1}:

$$M_V = 1.57(\pm 0.24) - 2.27(\pm 0.32)\log \times ((P/1\ \mathrm{hr})^{2/3}(L_X/L_{\rm edd})^{1/2}), \quad (1)$$

obtaining $M_V = 0.8 \pm 0.3$ (1σ error) for the optical counterpart. Among the 17 positionally consistent *HST* candidate optical/UV counterparts reported in Yukita et al. (2017), all but one are very similar to the surrounding stellar populations. The remaining source shows an excess in the blue band, making it an interesting potential counterpart of the accretion disk of an LMXB. From the blue apparent magnitude of the counterpart $m_B = 24.78$, standard extinction toward M31, and Equation (4) from Barnard et al. (2012), we obtain an absolute visual magnitude $M_V \simeq 0.3$. This is consistent (within 2σ) with the one derived from the X-ray luminosity and period of XMM0042, thus making it the likely optical counterpart.

The X-ray spectrum of XMM0042 (as seen by Yukita et al. 2017 and in this work) is quite hard, with $\Gamma \sim 1$ and $E_{\rm cutoff} \sim 18$ keV. This is consistent with what is seen in dipping LMXBs in our Galaxy, where a wide range of spectral properties is displayed, with photon indexes varying from 0.4 to 2 and cutoff energies from 3.5 to 80 keV (Diaz Trigo et al. 2006). The most luminous Galactic dipper, X 1624–490, has an X-ray luminosity in the 1–30 keV energy band of $\sim 7.3 \times 10^{37}$ erg s^{-1} (in the 0.5–50 keV energy range—Galactic dippers reach persistent luminosities only ~3 times lower than XMM0042; Balucinska-Church et al. 2000; Iaria et al. 2007) and a much softer spectrum.

The period, optical counterpart, and the spectrum of XMM0042 are reminiscent of a dipping LMXB system. The mean luminosity we found through our *XMM-Newton* analysis, ranging from 0.8 to 2.8×10^{38} erg s^{-1}, makes XMM0042 the most luminous dipper to date. Trudolyubov et al. (2002) found the first dipping source of M31, located in Bo 158. The period of the dipping behavior was 2.78 hr with a flux modulation of ~83%. A study of the other *XMM-Newton*, *Chandra*, and *ROSAT* observations (Trudolyubov & Priedhorsky 2004) revealed the amplitude of the dips to be anti-correlated with the source luminosity ($(0.5\text{–}2) \times 10^{38}$ erg s^{-1}), disappearing at high luminosities. The source also showed hour-timescale and month-timescale luminosity variations. This source has a rather hard spectrum, but it has never been observed by *NuSTAR*, so we have no information about the cutoff energy or its luminosity in the hard X-ray band. Another possibly dipping source in M31 was identified by Mangano et al. (2004), with a period of ~1.8 hr and a 0.3–10 keV luminosity of $\sim 10^{37}$ erg s^{-1}. In this case, however, a foreground X-ray source cannot be ruled out. We argue that we are observing the most luminous dippers in M31, the bright tail of their population in M31.

This research has made use of data produced by the EXTraS project, funded by the European Union's Seventh Framework Programme under grant agreement No. 607452. The EXTraS project acknowledges the usage of computing facilities at INAF's Astronomical Observatory of Catania. The EXTraS project acknowledges the CINECA award under the ISCRA initiative, for the availability of high performance computing resources and support.

Facility: XMM.

ORCID iDs

Martino Marelli https://orcid.org/0000-0002-8017-0338
Andrea Tiengo https://orcid.org/0000-0002-6038-1090
Andrea De Luca https://orcid.org/0000-0001-6739-687X
David Salvetti https://orcid.org/0000-0002-3853-5110
Luca Saronni https://orcid.org/0000-0002-1133-7632
Lara Sidoli https://orcid.org/0000-0001-9705-2883
Adamantia Paizis https://orcid.org/0000-0001-5067-0377
Ruben Salvaterra https://orcid.org/0000-0002-9393-8078
Andrea Belfiore https://orcid.org/0000-0002-2526-1309
Gianluca Israel https://orcid.org/0000-0001-5480-6438
Frank Haberl https://orcid.org/0000-0002-0107-5237
Daniele D'Agostino https://orcid.org/0000-0003-2649-0071

References

Balucinska-Church, M., Humphrey, P. J., Church, M. J., & Parmar, A. N. 2000, A&A, 360, 583
Barnard, R., Galache, J. L., Garcia, M. R., et al. 2012, ApJ, 756, 32
Barnard, R., Garcia, M. R., Primini, F., et al. 2014, ApJ, 780, 83

Bevington, P. R. 1969, Data Reduction and Error Analysis for the Physical Sciences (New York: McGraw-Hill)
De Luca, A., Salvaterra, R., Tiengo, A., et al. 2016, in The Universe of Digital Sky Surveys, Astrophysics and Space Science Proceedings, Vol. 42, ed. N. R. Napolitano et al. (Cham: Springer International), 291
Diaz Trigo, M., & Boirin, L. 2016, AN, 337, 368
Diaz Trigo, M., Parmar, A. N., Boirin, L., et al. 2006, A&A, 445, 179
Frank, J., King, A. R., & Lasota, J.-P. 1987, A&A, 178, 137
Hofmann, F., Pietsch, W., Henze, M., et al. 2013, A&A, 555, 65
Iaria, R., Lavagetto, G., DÁi, A., di Salvo, T., & Robba, N. R. 2007, A&A, 463, 289
Kong, A. K. H., Garcia, M. R., Primini, F. A., et al. 2002, ApJ, 577, 738
Mangano, V., Israel, G. L., & Stella, L. 2004, A&A, 419, 1045
Stanek, K. Z., & Garnavich, P. M. 1998, ApJ, 503, 131
Stiele, H., Pietsch, W., Haberl, F., et al. 2011, A&A, 534, 55
Trudolyubov, S., & Priedhorsky, W. 2004, ApJ, 616, 821
Trudolyubov, S. P., Borozdin, K. N., Priedhorsky, W. C., et al. 2002, ApJ, 581, 27
Van Paradijs, J., & McClintock, J. E. 1994, A&A, 290, 133
White, N. E., & Swank, J. H. 1982, ApJ, 253, 61
Wilms, J., Allen, A., & McCray, R. 2000, ApJ, 542, 914
Yukita, M., Ptak, A., Hornschemeier, A. E., et al. 2017, ApJ, 838, 47
Zechmeister, M., & Kurster, M. 2009, A&A, 496, 577